Research Article Vol. 34, No. 3 / 9 Feb 2026 / Optics Express 5459
Optics EXPRESS

Distributed refractive index sensing with cascaded TFBGs via derivative spectrum analysis

JIEQING ZHENG,[1] XUEHAO HU,[1] KARIMA CHAH,[1,2] AND CHRISTOPHE CAUCHETEUR[1,2,*]

[1]Advanced Photonic Sensors Unit, Department of Electromagnetism and Telecommunication, University of Mons, Mons 7000, Belgium
[2]WEL Research Institute, Avenue Pasteur, 6, 1300 Wavre, Belgium
[*]christophe.caucheteur@umons.ac.be

Abstract: Tilted fiber Bragg gratings (TFBGs) are highly sensitive refractometric probes, but their broad cladding-mode spectra have long been considered incompatible with wavelength-division multiplexing. As a result, TFBG refractive-index sensors are generally restricted to single-point operation, despite their inherent advantages. Here, we demonstrate for the first time that multiple bare, uncoated TFBGs (inscribed with distinct grating periods and tilt angles) can be cascaded within a single-mode fiber and independently interrogated over an 80-nm bandwidth. Although the cladding-mode spectra strongly overlap, we show that first-order derivative spectrum analysis isolates the local slope of each cut-off mode, effectively suppressing the envelope distortions typically induced by upstream gratings. This enables reliable and decoupled multipoint refractive-index sensing, with sensitivities of 52-58 nm/RIU that are fully consistent with intrinsic TFBG performance in aqueous media and remain stable after cascading. The derivative method enhances the demodulation accuracy by up to 65% and preserves linearity (R^2 = 0.94-0.98) while maintaining cross-talk below 0.03 nm. These results overturn the longstanding belief that TFBG refractometers cannot be multiplexed, paving the way for compact, low-cost, and scalable quasi-distributed chemical and biological sensing networks based on TFBG arrays.

1. Introduction

Tilted fiber Bragg gratings (TFBGs), first introduced by Erdogan and Sipe in the 1990s [1], have attracted considerable attention due to their unique ability to couple core-guided light into cladding modes. Unlike uniform FBGs, which reflect light at a narrow Bragg wavelength, TFBGs are usually inscribed with a small tilt angle (typically less than 10°) between the refractive index modulation planes and the perpendicular to the fiber axis. This structural asymmetry enables coupling from the core mode to a broad range of cladding modes, producing a rich transmission spectrum that is highly sensitive to changes in the surrounding refractive index (SRI) [2–4].

Among these spectral features, the cut-off mode, i.e. the cladding mode at the boundary beyond which the mode is no longer guided within the fiber's cladding, plays a critical role in TFBG-based SRI sensing. As the SRI increases, the cut-off wavelength redshifts due to changes in the effective refractive index of the cladding boundary, enabling highly sensitive and label-free detection of chemical or biological interactions at the fiber surface [5–7]. This mechanism has made TFBGs attractive for a variety of applications, including gas sensing [8], biosensing [9–11], and environmental monitoring [12–14].

TFBGs offer several advantages: high RI sensitivity of the order of tens nanometers per refractive index unit (RIU), the ability to support single-ended interrogation, and a broad spectral response with tens to hundreds of cladding-mode resonances. These properties have spurred

#585807 https://doi.org/10.1364/OE.585807
Journal © 2026 Received 25 Nov 2025; revised 7 Jan 2026; accepted 12 Jan 2026; published 5 Feb 2026

Optics EXPRESS

innovations in TFBG design, including coated gratings, multi-tilt configurations, and hybrid systems integrated with interferometers or resonators [15–17]. Functional coatings such as gold, graphene, or responsive polymers have further enhanced the selectivity and sensitivity of TFBGs to targeted analytes [18–20]. Additionally, the complex spectral content of TFBGs has enabled the use of advanced signal processing techniques, such as principal component analysis (PCA) and linear discriminant analysis (LDA), which are particularly suited for intelligent sensing platforms [21,22].

However, despite their sensing performances, TFBGs face practical limitations when it comes to multiplexing, especially in distributed sensing architectures. In contrast to uniform FBGs, which exhibit narrow reflection peaks (Full Width at Half Maximum (FWHM) usually between 0.15-0.6 nm) and are naturally compatible with wavelength-division multiplexing (WDM), TFBGs typically generate a broad cladding-mode spectrum spanning 70-80 nm, often occupying the entire usable bandwidth of a commercial optical interrogator [23–25]. As a result, most implementations are limited to one TFBG per optical channel, constraining the number of sensing points and increasing system complexity and cost. Early work on cascaded TFBG-based refractometric sensing was reported in [26], without overlap between the 3 TFBG amplitude spectra, enabling conventional wavelength-shift demodulation in an SRI range around 1.4.

In this work, we address this fundamental limitation by proposing a spectrally-engineered multiplexing strategy based on cascaded TFBGs with different periods and tilt angles, inscribed at different positions along a single-mode optical fiber. By carefully tuning the fundamental physical parameters of each grating, we control the cut-off wavelength of the cladding-mode coupling for each TFBG. This approach ensures that the cut-off mode positions of multiple gratings occupy non-overlapping segments of the interrogator bandwidth, allowing them to be simultaneously interrogated within a single optical channel. To enhance demodulation accuracy and minimize spectral interference, we apply first-order derivative spectrum analysis. This method improves the detection of small wavelength shifts and increases robustness against background variations, enabling reliable and independent SRI measurements at multiple locations along the fiber.

Hence, this study presents, for the first time, multiple TFBGs with strongly overlapping cladding-mode spectra are multiplexed within a single interrogation channel, and their individual refractive-index responses are independently recovered. Our approach retains the intrinsic advantages of TFBGs (high sensitivity, rich spectral information, and single-ended operation) while overcoming their longstanding multiplexing limitations. This architecture significantly reduces hardware requirements, lowers system cost, and opens the door to dense, real-time, and spatially resolved SRI monitoring in compact and integrated fiber-optic sensing networks.

2. Materials and methods

2.1. Grating inscriptions and fundamental principle

TFBGs were inscribed in a standard single-mode optical fiber (Corning SMF-28) with three different phase masks using a pulsed Excimer laser at 193 nm (Noria system from Northlab Photonics). The careful selection of dedicated phase masks with different periods and tilt angles can ensure a good distribution of the cut-off mode region for each TFBG within the interrogator bandwidth. The grating length was uniformly set to 10 mm. The main parameters of the three TFBGs used in this work are summarized in Table 1.

Table 1. Main parameters of the 3 TFBGs used in our experiments

# Grating	Period (nm)	Tilt angle (°)	Length (mm)
TFBG1	541.80	7	10
TFBG2	544.65	8	10
TFBG3	566.14	7	10

Optics EXPRESS

Different periods and tilt angles determine the coupling characteristics between the optical core mode and the different cladding modes. When the grating plane is tilted, the most obvious effect is the strong enhancement of the cladding mode resonances, in addition to the core mode coupling at the Bragg resonance. The relationships defining the resonance peak of the fiber core mode at the wavelength (λ_B) and the wavelength of the i^{th} cladding mode ($\lambda_{clad,i}$), are [27]:

$$\lambda_B = 2n_{core}^{eff}\frac{\Lambda}{\cos\theta} \tag{1}$$

$$\lambda_{clad,i} = (n_{core}^{eff} + n_{clad,i}^{eff})\frac{\Lambda}{\cos\theta} \tag{2}$$

where θ is the tilt angle of the grating plane with respect to the perpendicular to the axial direction of the optical fiber, n_{core}^{eff} is the effective RI of the core mode, $n_{clad,i}^{eff}$ is the effective RI of the i^{th} order cladding mode, and Λ is the grating period.

According to Eq. (2), the effective RI of each cladding mode directly affects its resonance wavelength, so the SRI can be accurately measured by monitoring the change of the cladding modes' effective RI.

2.2. Test procedure for refractometric sensing

To evaluate the response of each TFBG structure to variations in SRI, calibration measurements were conducted using a set of standard RI solutions. Ten LiCl-water mixtures were prepared to calibrate the refractometric response of the sensors. Lithium chloride fully dissociates in water ($LiCl \rightarrow Li^+ + Cl^-$), and therefore the solution concentrations are expressed in terms of LiCl molarity. The solutions were prepared using a standard dilution procedure based on the conservation of mass ($C_1V_1 = C_2V_2$). An initial stock solution was obtained by dissolving a known mass of LiCl in deionized water, followed by successive dilutions through progressive addition of water. The refractive index of each solution was measured using an Abbe refractometer at a wavelength of 589 nm, providing a measurement precision of 2×10^{-4} RIU. The resulting refractive indices ranged from 1.3331 to 1.3349, with an associated uncertainty not exceeding ±0.0002. The TFBG region of the optical fiber was sequentially immersed in each solution, allowing a stabilization period of one minute before spectral acquisition. TFBG amplitude spectra were recorded using an FBG interrogator and subsequently processed using a dedicated demodulation technique that enabled the accurate measurement of the cut-off mode shift. The resulting wavelength shifts were plotted as a function of RI, and linear regression analysis was performed to determine the sensor sensitivity and the coefficient of determination (R^2). This procedure was repeated for single, double and triple cascaded TFBGs configurations in order to compare their respective measurement accuracies and RI decoupling capabilities.

The experimental sensing setup is illustrated in Fig. 1. Two-pass transmission spectra were recorded in a single-ended configuration, where the Fresnel reflection at the flat-cleaved fiber-air interface (~4%) served as the return signal for the interrogator [28]. The tests were performed iteratively for different TFBG configurations subject to controlled variations in SRI, by immersing the bare grating region into calibrated LiCl-water solutions. First, TFBG1 was connected to the interrogation system, and its surrounding RI was varied ten times using calibrated LiCl-water solutions. Next, the cascade with TFBG1 and TFBG2 was tested. To investigate TFBG1 target, the RI around this grating was varied nine times starting from 1.3331 up to 1.3349. For each RI value around TFBG1, the RI around TFBG2 was varied across ten values, resulting in a total of 100 combinations of RI values. Afterwards, the roles were then reversed to investigate target TFBG2: the TFBG2 RI was varied (10 values in total), while for each RI value around TFBG2, the TFBG1 RI was varied (10 values in total), resulting in another total of 100 combinations of RI values. Finally, TFBG1, TFBG2 and TFBG3 were connected in cascade. The RI surrounding

Optics EXPRESS

TFBG1 and TFBG2 was fixed at 1.3331, while the RI of the solution around TFBG3 was varied ten times to complete the third configuration.

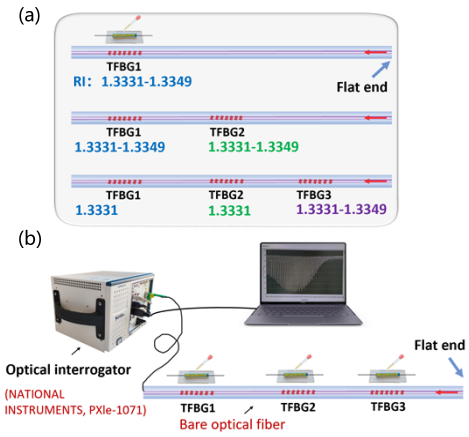

Fig. 1. (a) Design of experimental sensing schemes; (b) Schematic diagram of the experimental set-up used to interrogate the cascade of TFBGs.

For each configuration, the two-pass transmission amplitude spectra were recorded by optical interrogator (NATIONAL INSTRUMENTS, PXIe-1071) and the resonance wavelengths corresponding to each TFBG were extracted. Although the two-pass transmission spectra were used in this work, it is worth to recall that the sensing mechanism and refractive-index sensitivity were equivalent to those observed in transmission. As shown in Fig. 1(b), the system consists of three main components: (1) a TFBG array consisting of maximum 3 TFBGs, cascaded along a single optical fiber with a flat-cleaved end; (2) an FBG interrogator featuring a tunable laser source and a spectral resolution of 0.004 nm, used to capture the two-pass transmission spectra in the range 1510-1590 nm; and (3) a data processing unit, where the recorded spectra were analyzed in real time using a derivative-based algorithm, as explained hereafter.

During all the experiments, the ambient temperature was kept within the range of (22 ± 0.5) °C. The wavelength shift caused by temperature (≈10 pm/°C for silica) was negligible compared with the RI-induced spectral shift. For field applications, temperature compensation can be implemented using a reference grating [29].

Figure 2(a-c) show the individual two-pass transmission amplitude spectrum of TFBG1, TFBG2 and TFBG3, respectively, measured in the wavelength range [1510-1590 nm] when they were immersed in a 1.3331 RI solution. The cut-off mode region is highlighted in color for each grating and is respectively located around 1514, 1537 and 1577 nm. Figure 2(d) depicts the full spectrum corresponding to the 3 cascaded TFBGs. The spectral overlap is such that it becomes tricky to precisely locate the cut-off mode region, especially for TFBG2. Hence, the standard interrogation method based on the tracking of the cut-off mode wavelength shift [30] can no longer be applied and we had to consider another demodulation method, as explained in section 2.3 hereafter.

2.3. *Analysis method for derivative spectrum*

The first-order derivative technique is widely applied in spectral analysis to enhance feature visibility and extract fine variations in spectral profiles [31,32]. Given a spectral signal $I(\lambda)$, where λ denotes the wavelength and I the corresponding intensity, its first-order derivative is defined as:

$$\frac{dI(\lambda)}{d\lambda} = \lim_{\Delta\lambda \to 0} \frac{I(\lambda + \Delta\lambda) - I(\lambda)}{\Delta\lambda} \tag{3}$$

Optics EXPRESS

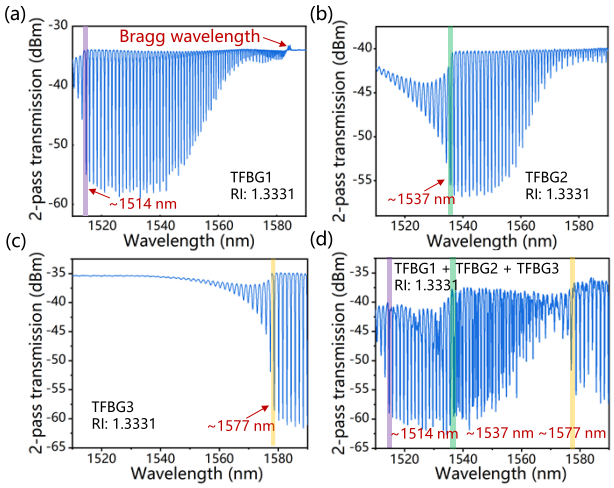

Fig. 2. Two-pass transmission amplitude spectrum of TFBG1 (a), TFBG2 (b), TFBG3 (c) and the cascade TFB1-TFBG2-TFBG3 (d), each immersed in a 1.3331 RI solution.

This expression quantifies the local rate of change in intensity with respect to wavelength and corresponds to the instantaneous slope of the spectral curve. In practice, the first-order derivative was computed numerically using a central finite-difference scheme applied to the uniformly sampled spectra delivered by the interrogator ($\Delta\lambda = 0.004$ nm), yielding a reliable estimation of the local spectral slope rather than a strict continuous derivative.

The first-order derivative signal exhibits positive values on rising edges, negative values on falling edges, and crosses zero at local extrema, thus enables accurate identification of peak positions. Furthermore, the derivative process effectively suppresses slowly varying baselines while amplifying subtle spectral features. These properties make it a powerful tool in applications such as multipoint peak detection, shoulder feature enhancement, and wavelength shift demodulation in fiber-optic sensing systems. Higher-order derivatives were also tested, but they amplified noise and introduced spectral distortion. The first-order derivative was therefore adopted, as it provides clear feature separation with minimal noise enhancement. We will see in the following that, because of the shoulder feature enhancement, it contributes to enhance the refractometric sensitivity of the probe.

3. Results and discussion

3.1. Surrounding RI measurements with TFBG1 using derivative method

To evaluate the advantages of the derivative method proposed in this work for RI measurements based on a cascade of TFBGs whose cladding mode resonances overlap, the spectrum response of TFBG1 was processed comparatively with different RI values (1.3331-1.3349). All sensitivities were calculated based on the wavelength of the selected spectral feature. Figure 3(a, b) show respectively the evolution of the two-pass transmission amplitude spectrum as a function of the surrounding RI value and a zoomed-in spectrum around the cut-off mode. The minimum of the latter can be reliably followed to find its central wavelength whose shift reflects well the changes in the surrounding RI values, as depicted in Fig. 3(e). The obtained sensitivity is 30.52 nm/RIU (refractive index unit), which is consistent with previously published results [33].

In contrast, the derivative method results shown in Fig. 3(c) and Fig. 3(d) clearly amplify the variation trend at the cladding mode edges. As illustrated in Fig. 3(f), the coefficient of determination R^2 is improved from 0.89 to 0.98, and the sensitivity is 50.34 nm/RIU increased

Optics EXPRESS

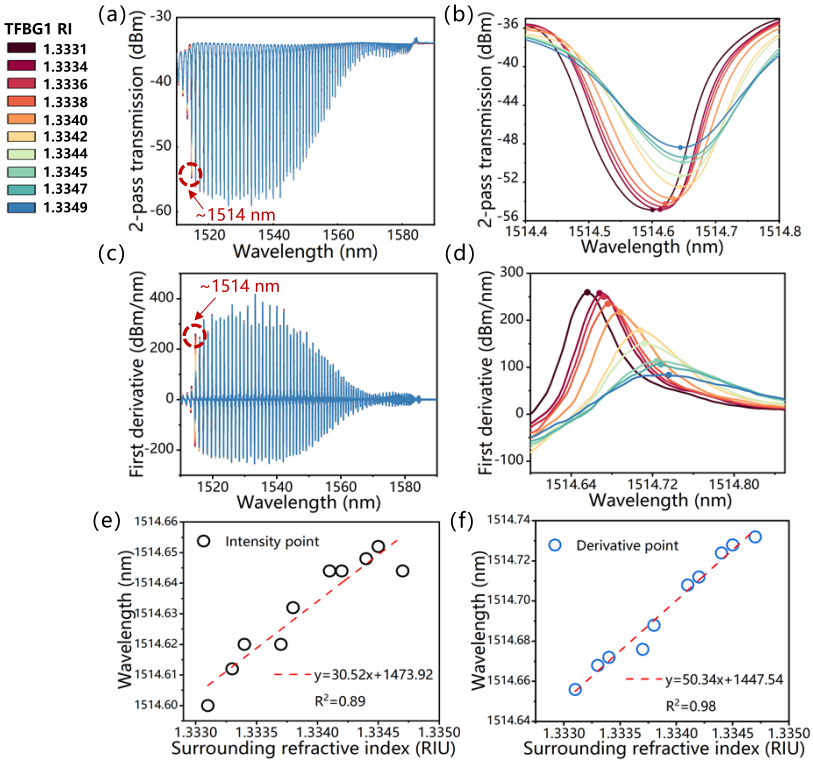

Fig. 3. (a) Evolution of the two-pass transmission amplitude spectrum of TFBG1 as a function of the surrounding RI value; (b) zoomed-in spectrum around the cut-off mode resonance; (c) evolution of the derivative of the two-pass transmission amplitude spectrum of TFBG1 as a function of the surrounding RI value; (d) zoomed-in derivative of the spectrum on the most sensitive region corresponding to the cut-off mode location; (e) wavelength of the cut-off mode resonance as a function of the surrounding RI value; (f) wavelength of the local maximum of the derivative-based demodulation method as a function of the surrounding RI value.

by approximately 65%. These results indicate that the derivative-based method effectively suppresses spectral fluctuations and enhances the detection of weak signals, making it more suitable for high-precision sensing applications [34,35].

While comparable sensitivities can be obtained without derivatives for a single isolated TFBG, derivative processing becomes essential in cascaded configurations, where overlapping spectral envelopes prevent reliable tracking of cut-off extrema using raw spectra.

3.2. *Surrounding RI measurements with TFBG1 and TFBG2 in cascade*

The system yielded a stable and representative composite two-pass transmission spectrum. For target TFBG1 and TFBG2 as a function of surrounding RI, two distinct regions (~1514 nm and ~1537 nm) of spectral variation emerge, as shown in Fig. 4(a) and Fig. 4(c), respectively. Furthermore, when the composite spectrum was processed using the first-order derivative spectrum analysis, as illustrated in Fig. 4(b) and Fig. 4(d), the variation trends of the cladding mode edges were significantly enhanced. Figure 4(e) and 4(f) present the locally enlarged region spectral around the cut-off mode of TFBG2, extracted from the corresponding original and derivative spectra. In Fig. 4(e), the two-pass transmission spectra show the gradual shift of

Optics EXPRESS

the cut-off resonance near 1537 nm as the surrounding refractive index increases from 1.3331 to 1.3349. Figure 4(f) displays the first-order derivative spectra of the same region, where the zero-crossing and peak features become more distinct with the derivative processing, allowing clear identification of the cut-off mode. These illustrations highlight the effectiveness of the first-order derivative method in resolving overlapped spectral features and confirm that the cut-off mode of TFBG2 is indeed captured in the measured data. This transformation enables clear distinction between previously overlapping spectral features, thereby improving the resolution of multipoint sensing.

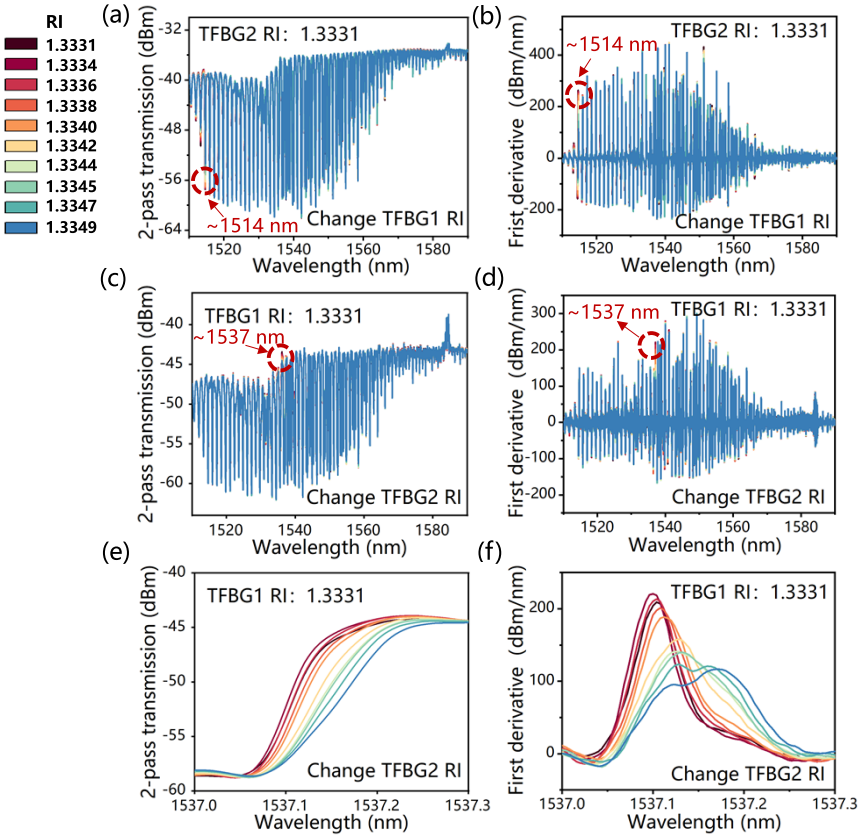

Fig. 4. Evolution of the two-pass transmission amplitude (a) and derivative (b) spectrum ~1514 nm of the TFBG1-TFBG2 cascade, as a function of the TFBG1 surrounding RI value (TFBG2 RI: 1.3331); evolution of the two-pass transmission amplitude (c) and derivative (d) spectrum ~1537 nm of the TFBG1-TFBG2 cascade, as a function of the TFBG2 surrounding RI value (TFBG1 RI: 1.3331) (e) enlarged region and (f) derivative spectral around the cut-off mode of TFBG2.

Specifically, the peaks of the derivative wavelengths of cut-off modes of TFBG1 and TFBG2 shift with increasing RI in the 1514.6-1514.8 nm and 1537.0-1537.3 nm bands, respectively. The two spectra do not overlap, clearly highlighting the effectiveness of the tilt-angle-based design in achieving spatial multiplexing.

The interference between TFBG1 and TFBG2 is investigated below. As shown in Fig. 5(a), the derivative of the two-pass transmission amplitude spectrum of TFBG1 around the cut-off ~1514 nm remained essentially stable with a maximum shift of less than 0.03 nm, when the

Optics EXPRESS

surrounding RI environment of TFBG2 was changed. This result demonstrates that dual-point measurements can be achieved within the same spectral channel with a high degree of independence and negligible cross-sensitivity. It confirms that the interference between TFBGs in the cascaded structure is minimal, enabling truly independent RI sensing at two locations. The refractometric response of TFBG1 around the cut-off ~1514 nm is shown in Fig. 5(b), with a sensitivity of 52.96 nm/RIU and a R^2 value exceeding 0.98 by linear regression.

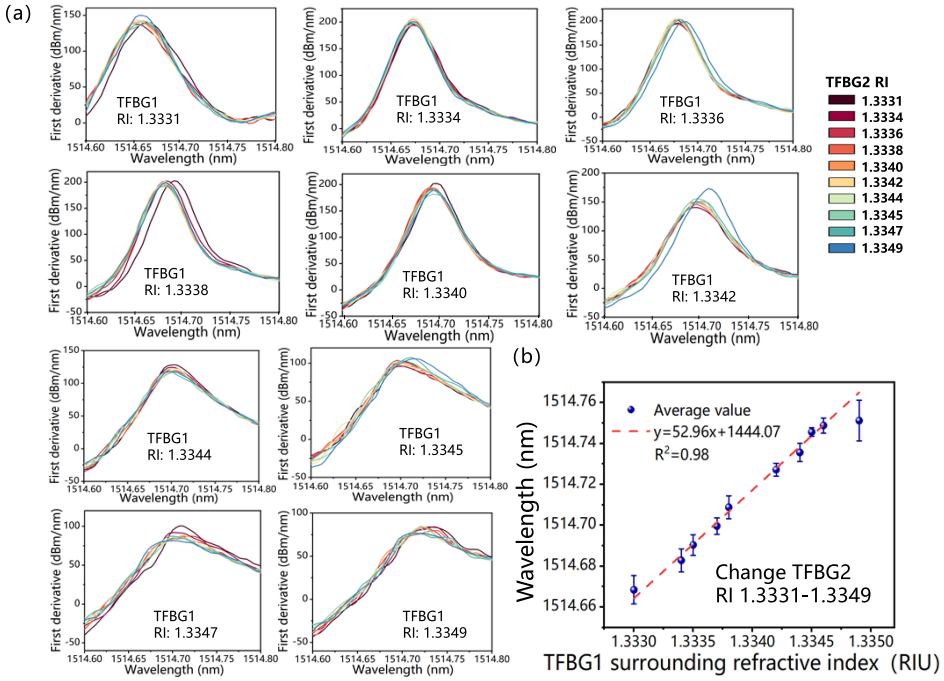

Fig. 5. (a) Derivative spectra of TFBG1 around the cut-off ~1514 nm at fixed RI values of TFBG1 and varying RI of TFBG2 between 1.3331-1.3349; (for each TFBG1's RI, TFBG2's RI changes from 1.3331 to 1.3349); (b) evolution of derivative spectral peak of TFBG1 around the cut-off ~1514 nm with varying TFBG1 RI between 1.3331-1.3349; the error bars represent the standard deviation (RMS value) of the extracted derivative-peak wavelength induced by varying the surrounding refractive index of the non-target TFBG2 over the full calibration range.

For target TFBG2, as shown in Fig. 6(a), although small fluctuations are observed, the induced wavelength variations remain limited (<0.04 nm) and significantly smaller than the RI-induced wavelength shift of the target grating, confirming negligible cross-talk, when the surrounding RI environment of TFBG1 was changed. Figure 6(b) presents the refractometric response of TFBG2 with a sensitivity of 54.25 nm/RIU and a R^2 value exceeding 0.94 after linear fit. For Fig. 5(b) and Fig. 6(b), the error bars were calculated as the standard deviation of the demodulated wavelength over all combinations of refractive-index variations applied to the non-target grating.

These results indicate that the two TFBGs exhibit negligible mutual interference when the RI of the other changes, demonstrating the feasibility of independent dual-point measurements. This enables simultaneous, independent multipoint RI monitoring within the same spectral window.

3.3. Surrounding RI measurements with TFBG1, TFBG2 and TFBG3 in cascade

Building upon the dual-TFBG cascade, a third grating (TFBG3) was introduced to form a three-point cascaded sensing system. As shown in Fig. 7(a), the two-pass transmission amplitude

Optics EXPRESS

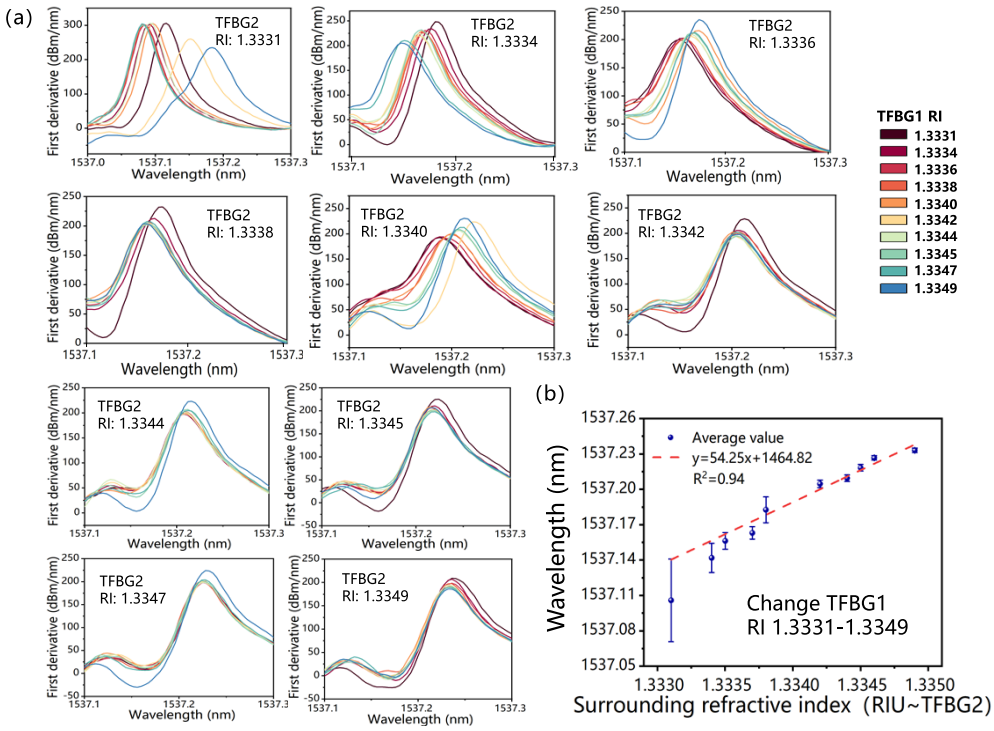

Fig. 6. (a) Derivative spectra of TFBG2 around the cut-off ~1537 nm for fixed values of TFBG2 RI and varying TFBG1 RI from 1.3331 to 1.3349; (b) evolution of derivative spectral peak of TFBG2 around the cut-off ~1537 nm with varying TFBG2 RI between 1.3331-1.3349; the error bars represent the standard deviation (RMS value) of the extracted derivative-peak wavelength induced by varying the surrounding refractive index of the non-target TFBG1 over the full calibration range.

spectrum response of the cascaded configuration when the surrounding RI of TFBG3 was varied from 1.3331 to 1.3349. The first-derivative spectra reveal a pronounced peak near 1578 nm with enhanced sensitivity and reduced spectral noise, facilitating accurate wavelength identification as illustrated in Fig. 7(b). Figure 7(c) shows the zoomed-in derivative curves around 1578 nm demonstrating a consistent shift as the TFBG3 surrounding RI value increases, without distortion of the peak profile. The peak wavelength extracted from the derivative spectrum exhibits an excellent linear relationship as the TFBG3 surrounding RI value increases ($R^2 = 0.97$), with a sensitivity of approximately 57.53 nm/RIU as shown in Fig. 7(d).

The influence of TFBG3 on the responses of TFBG1 and TFBG2 is minimal, resulting in wavelength shifts of less than 0.02 nm, as shown in Fig. 7(e) and Fig. 7(f). This shift accounts for less than 2% of the dominant mode's response range, validating both the stability and scalability of the system. The experimental results further confirm that the introduction of TFBG3 has a negligible effect on the around the cut-off wavelength sensing region of TFBG1 and TFBG2, demonstrating the feasibility of effective multiplexing. The derivative method enables clear extraction of the three individual response signals, thereby achieving accurate multi-point RI measurements.

Optics EXPRESS

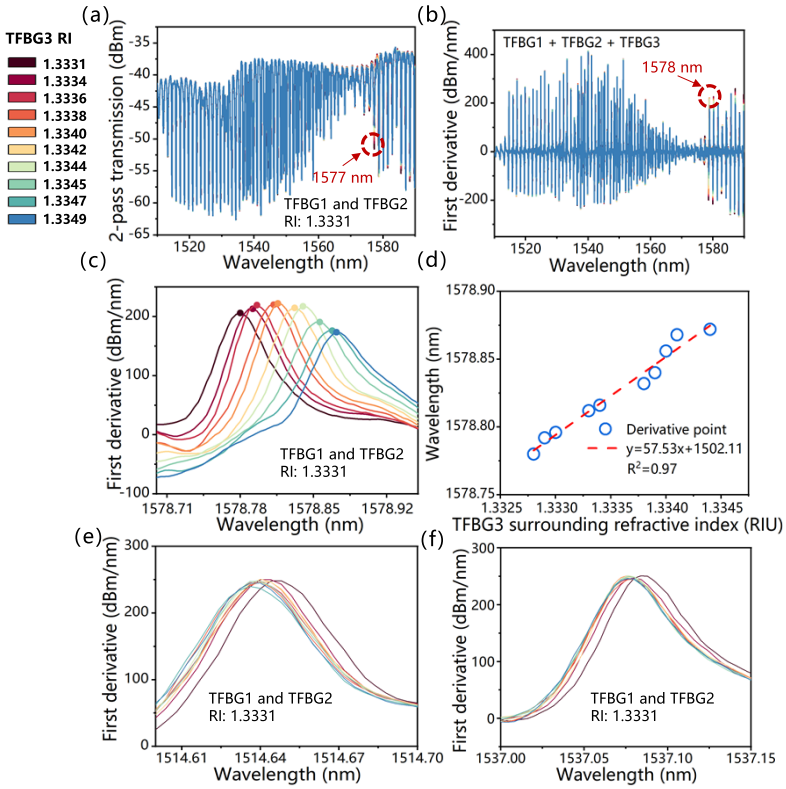

Fig. 7. (a) Evolution of the two-pass transmission amplitude spectrum as a function of the TFBG3 surrounding RI value; (b) evolution of the derivative of the two-pass transmission amplitude spectrum as a function of the TFBG3 surrounding RI value; (c) zoom around the derivative of the two-pass transmission amplitude spectrum; (d) linear fit of the derivative of the two-pass transmission amplitude spectrum; (e) in the TFBG1 around the cut-off ~1514 nm, and (f) in the TFBG2 around the cut-off ~1537 nm, evolution of the derivative of the two-pass transmission amplitude spectrum as a function of TFBG3 surrounding RI value.

3.4. Discussion

By precisely controlling the period and tilt angle of each grating, the cladding mode responses are effectively distributed across the wavelength domain, creating natural spectral separation. The derivative method further amplifies the variation at the edges of the cladding modes, thereby compensating for the sensitivity loss caused by spectral overlap in conventional intensity-based approaches. It should be emphasized that the proposed multiplexing strategy requires TFBGs with distinct grating parameters. Identical gratings producing overlapping cut-off modes cannot be discriminated and therefore cannot be multiplexed using this approach.

As summarized in Table 2, the sensing performance of the proposed quasi-distributed TFBG array remains stable and reliable after cascading multiple gratings along the same fiber. The single TFBG1 measurements show that the use of the first-order derivative enhances the fitting accuracy, with the linear correlation coefficient (R^2) improving from 0.89 to 0.98 and the sensitivity increasing from 30.52 nm/RIU to 50.34 nm/RIU. This improvement indicates that the derivative processing effectively suppresses baseline fluctuations and enhances the spectral discrimination of the cladding-mode resonances.

Optics EXPRESS

Table 2. Comparison of key sensing performance metrics before and after cascading, and with/without first-order derivative analysis

Sensor configuration	Processing method	Sensitivity (nm/RIU)	Linear correlation (R^2)	Noise level (nm)
Single TFBG1 (independent)	Raw spectrum	30.52	0.89	-
Single TFBG1 (independent)	1st-derivative	50.34	0.98	-
Cascaded TFBG1	1st-derivative	52.96	0.98	0.03
Cascaded TFBG2	1st-derivative	54.25	0.94	0.04
Cascaded TFBG3	1st-derivative	57.53	0.97	-

Compared with the tracking of the cut-off mode wavelength shift method, the derivative method offers advantages in the following three aspects: (1) Amplification of subtle changes: Spectral variations at the edges are significantly amplified after derivative processing, making the method well-suited for low-concentration detection. (2) Suppression of spectral drift: The influence of spectral power shifts on the fitting accuracy is reduced, thereby improving the linearity (R^2) of the response curves. (3) Enhanced spectral decoupling: The method facilitates the separation of closely spaced envelope modes, improving the system's ability to resolve multiple sensing points.

In the cascaded configuration, the sensitivity values for the three sensing points remain within the range of 52.96-57.53 nm/RIU, comparable to or slightly higher than those of the single TFBG measurement, demonstrating that mutual spectral interference among adjacent gratings is minimal. The linear fitting coefficients (R^2 = 0.94-0.98) confirm excellent linearity between the wavelength shift and the refractive index variation. Although amplitude-based interrogation can be considered, it is strongly affected by power fluctuations, polarization changes, and spectral distortions in cascaded configurations. In contrast, wavelength-based demodulation benefits from the high wavelength resolution of the interrogator (~0.004 nm) and the relatively large RI-induced wavelength shifts (~0.1 nm), resulting in a superior signal-to-noise ratio. The derivative-based wavelength tracking further suppresses baseline variations, making it particularly suitable for multiplexed TFBG systems with overlapping spectra.

The measured noise levels (0.03-0.04 nm) are low enough to ensure a high signal-to-noise ratio, corresponding to a refractive-index resolution better than 10^{-4} RIU. These results verify that the first-order derivative method enables accurate multi-point refractive-index interrogation in a single-fiber system without significant degradation in sensitivity or linearity after cascading.

Although TFBGs support a large number of cladding modes, the cut-off mode region concentrates the highest refractive-index sensitivity. Focusing on this single, well-defined feature enables accurate and repeatable SRI measurements while preserving multiplexing capability. It is important to note that the proposed demodulation strategy does not rely on tracking all individual cladding-mode resonances. Instead, a single derivative-based spectral feature associated with the cut-off region is used for each TFBG. This feature provides a monotonic and reproducible response to refractive-index variations and therefore enables straightforward calibration.

In practical operation, it is important to emphasize that the proposed demodulation approach is primarily intended for the detection of small refractive-index variations in aqueous solutions, as typically encountered in chemical and biological sensing applications.

Given the 80 nm interrogation bandwidth and the fact that each TFBG cut-off region requires approximately 8-10 nm of spectral allocation after derivative processing to ensure stable and decoupled demodulation, we believe that up to seven TFBGs can be multiplexed within a single optical channel. This estimate is intentionally conservative, as it accounts for spectral broadening, noise margins, and cross-talk suppression. For practical implementation, a general design strategy can be summarized as follows: (1) distinct grating periods should be selected to distribute the cut-off wavelengths across the available bandwidth; (2) moderate tilt angles (6-9°) should be

Optics EXPRESS

used to maintain strong cladding-mode coupling while limiting spectral congestion; (3) adjacent cut-off regions should be separated by at least ~10 nm. These guidelines provide a straightforward framework for designing scalable quasi-distributed TFBG sensing networks.

To further optimize the demodulation process in this case, future work could explore the integration of machine learning-based spectral fitting or wavelet decomposition techniques to enhance recognition accuracy and improve resistance to interference.

Finally, we believe that the first-order derivative method can also be applied to cascaded TFBG-SPR sensors to enhance spectral feature discrimination. In this case, optimization of the smoothing parameters, metal-film thickness, and grating tilt angle would be necessary to maintain spectral separability and measurement stability.

4. Conclusions

In this work, we have demonstrated a novel and practical approach to overcome one of the key limitations of TFBGs: their incompatibility with traditional multiplexing techniques. By cascading multiple TFBGs with distinct tilt angles and grating periods along a single-mode optical fiber, and by employing first-order derivative spectrum analysis, we successfully achieved simultaneous, independent, and reliable interrogation of multiple sensing points using a single optical channel, even in the presence of overlapping cladding-mode spectra.

This strategy enables quasi-distributed RI sensing without sacrificing the intrinsic strengths of TFBGs, such as their high sensitivity, rich spectral content, and single-ended interrogation capability. The proposed architecture not only simplifies system design and reduces hardware complexity and cost, but also opens the door to high-density, spatially resolved chemical and biological sensing in compact and integrated optical fiber platforms.

This work does not introduce the concept of cascaded TFBGs itself, but demonstrates for the first time that strongly spectrally superposed TFBGs can be independently interrogated for refractive-index sensing using derivative spectrum analysis. This overturns the conventional assumption that spectral overlap inherently prevents multiplexing of TFBG-based refractometers.

Future work will focus on extending this technique to longer arrays, exploring dynamic or in-situ applications in complex environments, and integrating functional coatings for enhanced selectivity. The demonstrated multiplexing scheme represents a significant advancement toward scalable, intelligent, and cost-effective TFBG-based sensing networks.

Funding. Fund for Scientific Research (F.R.S. – FNRS).

Acknowledgment. The author thanks the technical support of Mariel David.

Disclosures. The authors declare no competing interests.

Authors' contributions. J. Zheng conducted the experiments and the data analysis. He drafted the manuscript. K. Chah fabricated the TFBGs, revised the experiments and the manuscript. X. Hu assisted J. Zheng in the demodulation process and revised the manuscript. C. Caucheteur supervised the work and co-wrote the manuscript.

Data availability. All data are available upon request.

References

1. T. Erdogan and J. E. Sipe, "Tilted fiber phase gratings," J. Opt. Soc. Am. A **13**(2), 296–313 (1996).
2. C. Caucheteur, T. Guo, F. Liu, *et al.*, "Ultrasensitive plasmonic sensing in air using optical fibre spectral combs," Nat. Commun. **7**(1), 13371 (2016).
3. M. Lobry, M. Loyez, E. M. Hassan, *et al.*, "Multimodal plasmonic optical fiber grating aptasensor," Opt. Express **28**(5), 7539–7551 (2020).
4. A. Ortega-Gomez, M. Loyez, M. Lobry, *et al.*, "Plasmonic sensors based on tilted Bragg gratings in multicore optical fibers," Opt. Express **29**(12), 18469–18480 (2021).
5. S. Cięszczyk, "Application of Gabor, Log-Gabor, and Adaptive Gabor Filters in Determining the Cut-Off Wavelength Shift of TFBG Sensors," Appl. Sci. **14**(15), 6394 (2024).
6. X. Han, H. Zhong, K. Li, *et al.*, "Operando monitoring of dendrite formation in lithium metal batteries via ultrasensitive tilted fiber Bragg grating sensors," Light: Sci. Appl. **13**(1), 24 (2024).
7. W. Lin, W. Huang, Y. Liu, *et al.*, "Cladding Mode Fitting-Assisted Automatic Refractive Index Demodulation Optical Fiber Sensor Probe Based on Tilted Fiber Bragg Grating and SPR," Sensors **22**(8), 3032 (2022).

Optics EXPRESS

8. Z. Yang, X. Yan, B. Peng, *et al.*, "Ultrafast and reproducible fiber-optic hydrogen sensor via a tilted fiber grating with Pd/WO3 nanocoating," Photonic Sens. **15**(2), 250229 (2025).
9. T. Guo, F. Liu, B.-O. Guan, *et al.*, "[INVITED] Tilted fiber grating mechanical and biochemical sensors," Opt. Las. Technol. **78**, 19–33 (2016).
10. H. Fasseaux, M. Loyez, and C. Caucheteur, "Machine learning unveils surface refractive index dynamics in comb-like plasmonic optical fiber biosensors," Commun. Eng. **3**(1), 34 (2024).
11. S. Gao, X. Yang, S. Wang, *et al.*, "Review of optical fiber optofluidic chemical sensors and biosensors," Photonic Sens. **15**(1), 250134 (2025).
12. F. Liu, W. Lu, J. Huang, *et al.*, "Detangling electrolyte chemical dynamics in lithium sulfur batteries by operando monitoring with optical resonance combs," Nat. Commun. **14**(1), 7350 (2023).
13. H. Jean-Ruel and J. Albert, "Recent advances and current trends in optical fiber biosensors based on tilted fiber Bragg gratings," Trends Anal. Chem. **174**, 117663 (2024).
14. M. Lobry, M. Loyez, M. Debliquy, *et al.*, "Electro-plasmonic-assisted biosensing of proteins and cells at the surface of optical fiber," Biosens. Bioelectron. **220**, 114867 (2023).
15. B. Jiang, Z. Bi, S. Wang, *et al.*, "Cascaded tilted fiber Bragg grating for enhanced refractive index sensing," Chinese Phys. B **27**(11), 114220 (2018).
16. Y. Zhang, W. Bao, X. Zhu, *et al.*, "Research on lateral pressure sensing based on Sagnac ring cascaded FBG," Opt. Fiber Technol. **80**, 103423 (2023).
17. R. Zhang, S. Pu, Y. Li, *et al.*, "Mach-Zehnder interferometer cascaded with FBG for simultaneous measurement of magnetic field and temperature," IEEE Sens. J. **19**(11), 4079–4083 (2019).
18. C. Shen, Z. Huang, X. Chen, *et al.*, "Rapid ultra-sensitive nucleic acid detection using plasmonic fiber-optic spectral combs and gold nanoparticle-tagged targets," Biosens. Bioelectron. **242**, 115719 (2023).
19. H. Qu, S. Ma, C. Marques, *et al.*, "TFBGs in polyimide-coated optical fibers for multi-parameter measurements," Opt. Express **33**(14), 29322–29336 (2025).
20. X. Hu, Y. Liu, H. Wei, *et al.*, "Tilted Bragg grating in a glycerol-infiltrated specialty optical fiber for temperature and strain measurements," Opt. Lett. **49**(11), 2869–2872 (2024).
21. S. Cięszczyk and D. Harasim, "Polarization influence on algorithms of TFBG sensors data analysis for bending application," Appl. Sci. **13**(21), 11701 (2023).
22. M. Lobry, H. Fasseaux, M. Loyez, *et al.*, "Plasmonic fiber grating biosensors demodulated through spectral envelopes intersection," J. Lightwave Technol. **39**(22), 7288–7295 (2021).
23. C. Crunelle, C. Caucheteur, M. Wuilpart, *et al.*, "Quasi-distributed temperature sensor combining Fibre Bragg Gratings and temporal reflectometry technique interrogation," Opt. Lasers Eng. **47**(3-4), 412–418 (2009).
24. H. Qu, Z. Chen, S. Gao, *et al.*, "Femtosecond laser line-by-line tilted Bragg grating inscription in single-mode step-index TOPAS/ZEONEX polymer optical fiber," Opt. Lett. **48**(6), 1438–1441 (2023).
25. D. Harasim and P. Kisala, "Application of cascaded TFBG for wavelength-shift-based SRI measurement with reduced polarization cross-sensitivity," Sensors **25**(6), 1831 (2025).
26. M. D. Baiad and R. Kashyap, "Concatenation of surface plasmon resonance sensors in a single optical fiber using tilted fiber Bragg gratings," Opt. Lett. **40**(1), 115–118 (2015).
27. J. Albert, L. Y. Shao, and C. Caucheteur, "Tilted fiber Bragg grating sensors," Laser Photonics Rev. **7**(1), 83–108 (2013).
28. B. Lee, "Review of the present status of optical fiber sensors," Opt. Fiber Technol. **9**(2), 57–79 (2003).
29. A. D. Kersey, M. A. Davis, H. J. Patrick, *et al.*, "Fiber grating sensors," J. Lightwave Technol. **15**(8), 1442–1463 (1997).
30. C.-F. Chan, C. Chen, A. Jafari, *et al.*, "Optical fiber refractometer using narrowband cladding-mode resonance shifts," Appl. Opt. **46**(7), 1142–1149 (2007).
31. P. Santos, J. Almeida, and L. Coelho, "Study of LSPR spectral analysis techniques on SPR optical fiber sensors," U. Porto J. Eng. **8**(3), 12–17 (2022).
32. S. P. Chen, S. M. Taylor, S. Huang, *et al.*, "Application of odd-order derivatives in Fourier transform nuclear magnetic resonance spectroscopy toward quantitative deconvolution," ACS Omega **9**(34), 36518–36530 (2024).
33. S. Korganbayev, M. Sypabekova, A. Amantayeva, *et al.*, "Optimization of cladding diameter for refractive index sensing in tilted fiber Bragg gratings," Sensors **22**(6), 2259 (2022).
34. S. Cieszczyk, K. Skorupski, M. Wawrzyk, *et al.*, "A wavelet derivative spectrum length method of TFBG sensor demodulation," Sensors **23**(4), 2295 (2023).
35. Z. Huang, N. Yang, J. Xie, *et al.*, "Improving accuracy and sensitivity of a tilted fiber Bragg grating refractometer using cladding mode envelope derivative," J. Lightwave Technol. **41**(13), 4123–4129 (2023).